The Cryosphere Discuss., 1, 123–168, 2007
www.the-cryosphere-discuss.net/1/123/2007/

The Cryosphere Discussions

The Cryosphere Discussions is the access reviewed discussion forum of *The Cryosphere*

Reconstruction of the 1979–2006 Greenland ice sheet surface mass balance using the regional climate model MAR

X. Fettweis[1]

[1]Institut d'Astronomie et de Géophysique Georges Lemaître, Université catholique de Louvain, Louvain-la-Neuve, Belgium.

Received: 18 June 2007 – Accepted: 27 June 2007 – Published: 3 July 2007

Correspondence to: X. Fettweis (fettweis@astr.ucl.ac.be)

Abstract

Results from a 28-year simulation (1979–2006) over the Greenland ice sheet (GIS) reveal an increase of the solid precipitation ($+0.4\pm2.5\,km^3\,yr^{-2}$) and the run-off ($+7.9\pm3.3\,km^3\,yr^{-2}$) of surface melt water. The net effect of these competing factors leads to a significant Surface Mass Balance (SMB) loss rate of $-7.2\pm5.1\,km^3\,yr^{-2}$. The contribution of changes in the net water vapour fluxes ($+0.02\pm0.09\,km^3\,yr^{-2}$) and rainfall ($+0.2\pm0.2\,km^3\,yr^{-2}$) to the SMB variability is negligible. The melt water supply has increased because the GIS surface has been warming up +2.4°C since 1979. Latent heat flux, sensible heat flux and net solar radiation have not varied significantly over the last three decades. However, the simulated downward infra-red flux has increased by $9.3\,W\,m^{-2}$ since 1979. The natural climate variability (e.g. the North Atlantic Oscillation) does not explain these changes on the GIS. The recent global warming, due to the greenhouse gas concentration increase induced by the human activities, could be a cause of these changes. The doubling of the surface melt water flux into the ocean over the period 1979–2006 suggests that the overall ice sheet mass balance has been increasingly negative, given the probable meltwater-induced outlet glacier acceleration. This study suggests that an increased melting dominates over an increased accumulation in a warming scenario and that the GIS would likely continue to loose mass in the future. A GIS melting would have an effect on the stability of the thermohaline circulation (THC) and the global sea level rise.

1 Introduction

There is almost no more doubt now that human activities are responsible for a large part of the global temperature rise observed since the beginning of the industrial era. This is mainly due to increasing greenhouse gas (GHG) emissions (Solomon et al., 2007). Consequences of a warmer climate on the Greenland Ice Sheet (GIS) mass balance will be a growth in thickness inland, due to increased solid precipitation and

a perifical ice sheet thinning, due to a combination of an increasing surface melt and a likely induced increase of the iceberg discharge into the ocean along the coasts. Indeed, a temperature increase induces a larger melt of the snow/ice in summer but also a greater evaporation above the ocean which sends more moisture inland and consequently enhances precipitation. However, the increasing precipitation combined with a warming suggests a simultaneous competing increase in summer rain, which accelerates the snow/ice melting. With higher temperatures, more of the precipitation at low elevations will be rain instead of snow and the induced wetting of the snow leads to a reduced surface albedo, which can contribute to an earlier than normal onset of melt. The run-off of the meltwater represents about half of the annual mass loss of the GIS (Zwally and Giovinetto, 2001). The remainder of the ablation results mainly from iceberg discharge and subglacial melting (Reeh et al., 1999). The surface water vapour fluxes are generally small in comparison with precipitation rates (Box ans Steffen, 2001; Box et al., 2004). Finally, as recent observations suggest (Rignot and Kanagaratnam, 2006), the mass lost from discharge of icebergs could also increase as a consequence of global warming. Indeed, the recent acceleration of Greenland outlet glacier velocity (Howat et al., 2005; Luckman and Murray, 2005, 2006) could be associated to the increasing supply of meltwater reaching the glacier bed which, by lubrificating the ice/bedrock interface, facilitates the glacier sliding (Zwally et al., 2002). This will also lead to a thining of the margin and cause the ice sheet retreat from the coast as pointed out by Krabill et al. (1999). Due to the well known albedo and elevation feedbacks, a progressive depletion of the GIS would amplify the deglaciation (Ridley et al., 2005).

The increase in run-off is expected to exceed the precipitation increase (Alley et al., 2005; Lemke et al., 2007) and consequently, the GIS is likely to loose mass. If the GIS melts, the resulting freshwater increase could, on the one hand, perturb the thermohaline circulation (THC) by reducing the density contrast driving the THC (Rahmstorf et al., 2005), and on the other hand, contribute to the sea level rise (Dowdeswell, 2006) under the projected global warming (Solomon et al., 2007). Recent observation-based

studies show a significant surface melt increase over the GIS (Fettweis et al., 2007), a thinning at the margins (Krabill et al., 1999, 2004; Thomas et al., 2006), an increased discharge from outlet glaciers (Rignot et al., 2004; Rignot and Kanagaratnam, 2006) and a growing of the ice sheet in the Greenland interior (Krabill et al., 2000; Thomas et al., 2001; Thomas et al., 2006). The recent GIS observations made by laser altimeter and by NASA Gravity Recovery and Climate Experiment (GRACE) satellites rather suggest that the whole ice sheet is losing mass (Velicogna and Wahr, 2005; Chen et al., 2006; Luthcke et al., 2006; Thomas et al., 2006) while this trend is not unanimous (Johannessen et al., 2005; Zwally et al., 2005). However, these observation-based studies are not always representative for long-term values given the important year to year variations observed in the annual mass balance (Greuell et al., 2001; Howat et al., 2007). Therefore, large uncertainties remain in observation-based studies due to the sparse resolution of measurements in time and/or space and continued monitoring is needed to identify any significant future changes on the GIS (Lemke et al., 2007).

Numerical models provide an unique opportunity to fill this space-time gap over the GIS by determining more efficiently the whole ice sheet current mass balance evolution over longer periods (Hanna et al., 2005; Box et al., 2006). Among them, the high resolution limited-area Regional Climate Models (RCMs) nested in observation-based reanalysis offer the possibility to estimate the mass balance at spatial resolutions identical to satellite observations, by using sophisticated atmospheric physics and surface parametrizations designed for polar regions. They can be thought of as being physically-based interpolators of the assimilated observations (surface weather stations, atmospheric sounding and satellite remote sensing). That is why the GIS SMB is more and more studied with RCMs (Dethloff et al., 2002; Hanna et al., 2002; Box and Rinke, 2003; Mote, 2003; Box et al., 2006; Fettweis et al., 2006).

In order to improve predictions of the future behaviour of the GIS in the global warming context, it is necessary to better know and assess its current state and variability. That is the reason why we have chosen in this article to simulate the GIS SMB of the last thirty years with a coupled atmosphere-snow RCM having a horizontal resolution

of 25 km. The model used is the regional climate model MAR (Modèle Atmosphérique Régional) developed by Gallée and Schayes (1994). This model has already shown its capability on the GIS (Lefebre et al., 2003; Lefebre et al., 2005; Fettweis et al., 2005; Fettweis et al., 2006; Fettweis et al., 2007). The effective simulation starts in 1979 together with the beginning of remote sensing observations and lasts till the end of 2006. Any RCM applications to the past rather than the future benefit from the observations to drive the model (via the reanalysis) and to evaluate the model results afetrwords. Furthermore, our simulation illustrates the GIS response to the rapid warming observed on Greenland since the mid-1980's (Chylek et al., 2006, Box and Cohen, 2006). Finally, this 28-year simulation is one of the longest simulation known by the author of the Greenland climate made with a coupled snow atmospheric regional climate model until now (Box et al., 2006; Fettweis et al., 2007).

After a brief description of the RCM used in Sect. 2, Sect. 3 analyses in details the evaluation of the SMB simulated by MAR and its interannual fluctuations over the 1979–2006 period. The MAR model shows significant changes in the variability of the GIS SMB components since 1979. The atmospheric part of the MAR model helps us to better understand these changes in Sect. 4 where the surface energy balance over the GIS is discussed. Links with the North Atlantic Oscillation (NAO) are explored in Sect. 5 but the natural variability does not explain the simulated changes. The recent global warming due to increased greenhouse gas concentration could be at the root of these changes as concluded in Sect. 6.

2 The MAR model description

The model used here is the regional climate model MAR coupled to the 1-D Surface Vegetation Atmosphere Transfer scheme SISVAT (Soil Ice Snow Vegetation Atmosphere Transfer). The atmospheric part of MAR is fully described in Gallée and Schayes (1994), while the SISVAT scheme is detailed in De Ridder and Gallée (1998). The snow-ice part of SISVAT, based on the CEN (Centre d'Etudes de la Neige) snow

model called CROCUS (Brun et al., 1992), is an one-dimensional multi-layered energy balance model that determines the exchanges between the sea ice, the ice sheet surface, the snow-covered tundra, and the atmosphere (Gallée et al., 2001). It consists of a thermodynamic module, a water balance module taking into account the refreezing of the meltwater, a turbulence module, a snow metamorphism module, a snow/ice discretization module and an integrated surface albedo module. The blowing snow model, currently in development on the Antarctic ice sheet (Hubert Gallée, personal communication), is not yet used here. Despite the contribution of the wind snow erosion to the SMB variability seems to be low on the GIS (Box et al., 2004, 2006), it would be very interesting in the future to test this module on the GIS. In addition, the SISVAT does not contain an ice dynamics module. We thus only present the SMB and not the Ice sheet Mass Balance (IMB) of the GIS. Therefore, a fixed ice sheet mask to simulate the current climate is assumed.

The simulation starts in September 1977 (to reduce the impacts of the snow model initialization in 1979) and lasts till December 2006 with a spatial resolution of 25 km and a time step of 120 s. The ERA-40 reanalysis (1977–2002) and after that, the operational analysis (2002–2006) from the European Centre for Medium-Range Weather Forecasts (ECMWF) are used to initialize the meteorological fields at the beginning of the simulation in September 1977 and to force the lateral boundaries with temperature, specific humidity and wind components during the simulation. The (re)analysis is available every 6 h at a resolution of one degree (~100 km). The Sea Surface Temperatures (SST) and the sea-ice extent in the SISVAT module are also prescribed by the reanalysis. No corrections/calibrations are applied to the outputs of the model. The schemes and the set-up used here are fully described in Fettweis et al. (2005) and Lefebre et al. (2005).

3 The Greenland surface mass balance

3.1 Average annual rates of the SMB components

All the models listed in Table 1 agree unanimously to give an annual total ice sheet mass snowfall rate of ~600 $km^3\,yr^{-1}$. The net erosion by surface water vapour fluxes is estimated to be ~50–100 $km^3\,yr^{-1}$ (except by the MAR model) which gives an accumulation rate (usually noted P−E) of approximatively 550 $km^3\,yr^{-1}$. The MAR simulated annual snowfall and net surface water vapour fluxes are respectively plotted in Figs. 1a and 2a. The MAR solid precipitation exhibits recognized spatial patterns found from interpolation of ice core and snow pit data (e.g., Ohmura et al., 1999; Cogley, 2004) or simulated by models (e.g., Hanna et al., 2002, 2006; Box et al., 2006). See Fettweis et al. (2005) for more details about the validation of the MAR precipitation.

Unlike other models, the deposition/condensation accumulation simulated by MAR nearly dominates the sublimation/evaporation erosion in average over the whole ice sheet (see Table 1). Except at the summit where the small gain of mass modelled by MAR is consistent with the GC-Net observations, MAR underestimates the mass loss resulting from sublimation/deposition by comparison with the Polar MM5 outputs (Box et al., 2006) and the Box ans Steffen (2001) estimates based on GC-net observations (see Fig. 2a). This problem will be investigated in the future by reviewing the turbulence scheme used in the GIS simulations with MAR.

The run-off is estimated to be ~300 $km^3\,yr^{-1}$ (except by the ECHAM4 and MIT models), which gives an estimation of the SMB around 300 $km^3\,yr^{-1}$ balancing the glacier discharge and basal melting rate estimated by Reeh et al. (1999). Their glacier discharge estimation represents a minimum value in the current climate according to Box et al. (2006) because they do not account for for the melt-induced outlet glacier acceleration observed by Zwally et al. (2002). The larger run-off rate simulated by the Polar MM5 model could be partly explained by the discrepancies in the used ice sheet mask i.e. in the classification of ice/land/ocean land surface type. Along the south-eastern coast, the MM5 ice sheet margin runs directly along the sea, which increases signif-

icantly the melt overall. In other ice sheet masks (Mote, 2003; Fettweis et al., 2005; Hanna et al., 2005), there are tundra grid points between the ice sheet margin (which is higher in altitude as a result) and the sea. However, the MM5 SMB estimation is also the only model taking into account the snow erosion by the wind. The ECHAM4 and MIT models underestimate the ablation rate due to the absence of run-off along the northern coast of the ice sheet according to Bugnion and Stone (2002).

While the MAR model underestimates the sublimation/evaporation mass loss, it is consistent with other models by giving a SMB rate of 308 $km^3\ yr^{-1}$. In addition, the MAR patterns shown in Fig. 3a fully agree with other estimations based on both observations (Zwally and Giovinetto, 2001) and models (Box et al., 2004, 2006; Hanna et al., 2005) The MAR sublimation/evaporation underestimation can be assumed to be systematic each year. Therefore, it is reasonable to suppose that it weakly affects the temporal variability of the components simulation and that the MAR results can be used in a reliable way to study the SMB components evolution over the last 28 years. However, the accuracy of our model needs to be improved in the future to produce more reliable assessments of surface mass budget terms and their temporal changes.

3.2 Temporal variability and trend of the SMB components

The SMB is governed, on the one hand by accumulation (snowfall) and on the other hand, by run-off (temperature). The interannual variability in precipitation and ablation causes SMB fluctuations (with a correlation of 0.71 and respectively −0.90, see Fig. 4). In 1985, the SMB rate is abnormally low mainly because of low snowfall (see Table 2). Other SMB minima, rather due to a high fresh water flux into the ocean, are found in 1998 and 2003 in agreement with the Hanna et al. (2007) estimations. The absolute minimum of the SMB is reached in 2006 due to high run-off and very poor snowfall. Maxima of SMB occur on the one hand, in 1983 and 1992 after the volcanic eruptions from El Chichon and the Mount Pinatubo inducing a cooling and low melt rates. On the other hand, in 1996, owing to both negative run-off and positive snowfall anomalies, the SMB reaches a positive record rate as in Hanna et al. (2007). Integrated over the

ice sheet, the 28-year snowfall rate shows a positive trend of $+0.4\pm2.5\,km^3\,yr^{-2}$ (with a significance of 25%). The run-off increase is evaluated to be $+7.9\pm3.3\,km^3\,yr^{-2}$ (with a significance of 98%) which gives a rate of global average sea level rise of $(+2.2\pm0.9)\times10^{-2}\,mm\,yr^{-2}$. The computation was made by using an area of the world ocean of 361 million km^2. Error bars denote two standard deviations of the trend (i.e. a significance of 95%). This standard deviation has been calculated following Snedecor and Cochran (1971) using the method described in their Chapter 6.2. The net effect of these competing factors lead to a significant (95%) SMB mass loss rate of $-7.2\pm5.1\,km^3\,yr^{-2}$. The contribution of changes in the net water vapour fluxes to the SMB variability is negligible ($+0.02\pm0.1\,km^3\,yr^{-2}$) in agreement with Box et al. (2006). As shown in Figs. 4e and f, the heavier precipitation in the accumulation zone partly offsets the significant melt increase in the ablation zone. Indeed, the SMB variability shows an insignificant positive trend above 2000 m ($+0.7\pm1.7\,km^3\,yr^{-2}$) against a significant negative trend of $-7.8\pm4.0\,km^3\,yr^{-2}$ below 2000 m.

Over the 1979-2006 (resp. 1992–2003) period, MAR simulates a GIS mean surface elevation decrease of $-9\pm8\,mm\,yr^{-1}$ (resp. $-29\pm34\,mm\,yr^{-1}$). Patterns are shown in Fig. 5 and changes simulated by MAR below/above 1500 m/2000 m are summarized in Table 3. Only the decreases below 1500/2000 m are significant. These results are fully consistent with recent observations of surface elevation changes from satellite and aircraft altimeter shown in Table 3 (Johannessen et al., 2005; Zwally et al., 2005; Thomas et al., 2006). The agreement is best with the last available observations derived estimations from Thomas et al. (2006) showing also a GIS surface elevation decrease over the 1993–2004 period. Previous ERS satellite radar altimeter estimates showing rather a GIS elevation increase are in disagreement with other studies (e.g. Velicogna and Wahr, 2005; Chen et al., 2006; Luthcke et al., 2006) and need therefore to be considered with caution as discussed by (Thomas et al., 2006). In addition, the interannual variability is very high and 12-year long data set remains yet too brief to establish long-term trends.

The melt increase occurs everywhere along the ice sheet margin (Fig. 6b) according

to the GIS warming shown in Fig. 7a. The warming is larger above the ice sheet than along the ice sheet margin given that the surface temperature of melting snow/ice is limited to 0°C. The higher positive snowfall trend occurs near the south-eastern snowfall maximum (Fig. 1b) and negative trends are found along the ice sheet margin (lower in altitude). These negative trends are partly explained by the warming, which leads to an increase in the amount of liquid precipitation versus solid precipitation (Fig. 8b). These changes increase the melt water supply and have also consequences for glacier flow lubrication according to Zwally et al. (2002). Finally, Fig. 1c shows that the snowfall at Summit is an excellent indicator of the total ice sheet snowfall variability which fully justifies the choice of this location for ice-core Greenland climate reconstructions. Given that the melt increases everywhere, positive trends in the SMB occur only in the extreme South of the GIS where snowfall increases and dominates over the ablation (Fig. 3b). MAR simulates negative 28-year SMB trends almost everywhere in the ablation zone (in red in Fig. 3a) and a significant positive SMB trend in the south-eastern of the GIS. Figure 3c fully justifies SMB measurements near the K-Transect (in the South-East ablation zone) as records of the total GIS SMB variability Greuell et al. (2001).

The summer temperature exhibits a robust correlation with the melt water supply and therefore with the run-off (0.86) of the ice sheet as a whole (Fig. 9). This provides the basis for degree-day models. Heavier rainfall increases also the liquid water supply. It is true that the fraction of liquid precipitation is increasing on the GIS ($+0.2\pm0.2\,\mathrm{km^3\,yr^{-2}}$) but it does explain no more than 5% of the positive run-off 28-year trend estimated by MAR ($+7.9\pm3.2\,\mathrm{km^3\,yr^{-2}}$). The large part of the run-off acceleration is explained by the warming estimated by MAR to be $0.09\pm0.04\,^{\circ}\mathrm{C\,yr^{-1}}$. According to (Box et al., 2004), these considerations allow us to estimate the SMB anomaly for the entire ice sheet from the annual (yr) and June–July–August (JJA) temperature and the snowfall anomalies despite that these are not correlated. We have then:

$$\Delta \mathrm{SMB}_{\mathrm{GIS}} = -64.77\Delta T_{\mathrm{GIS}}{}^{\mathrm{yr}} + 1.57\Delta SF_{\mathrm{GIS}}{}^{\mathrm{yr}} \quad (1)$$

$$\Delta SMB_{\mathrm{GIS}} = -69.36\Delta T_{\mathrm{GIS}}{}^{\mathrm{JJA}} + 1.19\Delta SF_{\mathrm{GIS}}{}^{\mathrm{yr}} \quad (2)$$

where ΔSMB_{GIS} is the annual GIS SMB anomaly in km^3, ΔT_{GIS} is the annual (resp. JJA) GIS 3 m-temperature anomaly in °K and ΔSF_{GIS} is the annual GIS snowfall anomaly in km^3. The correlation (r) and the root mean square error (RMSE) between the SMB simulated anomaly and the SMB estimated anomaly are r=0.91 and RMSE=50.3 km^3 (resp. r=0.96 and RMSE=34.33 km^3). Such correlations confirm our hypothesis about the acute sensitivity to the SMB to both temperature and snowfall anomalies. If we use only the JJA temperature (in °K) and the annual snowfall anomalies (in mmWE) taken at Summit (the pixel used here has a latitude of 72.52° N, a longitude of 38.50° W and an altitude of 3232 m) to estimate the annual GIS SMB anomaly (in km^3),

$$\Delta SMB_{GIS} = -73.29 \Delta T_{Summit}{}^{JJA} + 1.90 \Delta SF_{Summit}{}^{yr} \quad (3)$$

the correlation remains very high (r=0.91 and RMSE=52.35 km^3) which suggests that the records at Summit are very good proxies of the current SMB variability. Finally, the annual SMB (in mmWE) simulated near the JAR-1 automatic weather station (the pixel used here has a latitude of 69.33° N, a longitude of 49.59° W and an altitude of 734.1m) shows a very good correlation with the annual GIS SMB (in km^3):

$$\Delta SMB_{GIS} = -0.12 \Delta SMB_{JAR-1}{}^{yr} \quad (4)$$

where r=0.91 and RMSE=37.0 km^3. Figure 3 shows the locations quoted in the text.

3.3 The equilibrium line altitude

The Equilibrium Line Altitude (ELA) is defined as the elevation where the SMB equals zero. Therefore, the ELA provides an useful indicator of the combined influence of thermal and precipitation forcing on the SMB. Our results (see Fig. 10) are in good agreement with Zwally and Giovinetto (2001) parametrisation. The general pattern is obviously an ELA decrease with increasing latitude. Regional variation in the ELA versus latitude pattern results from changes in local topography and precipitation regimes due to the proximity or not of dominant cyclonic systems. The relatively weak ELA at

61° N results, for example, from abundant snowfall observed in this region (see Fig. 1a). The trends for these last 28 years is a positive shift of +4.9 m yr^{-1} (resp. +12.6 m yr^{-1}) of the western (resp. eastern) Greenland ELA. This positive shift in altitude of the equilibrium line occurs everywhere (in red in Fig. 10) except at 62° N in the western Greenland which is the only region where the SMB is increasing (see Fig. 3b). These results corroborate the dominance of the thermal factors variability on the SMB.

3.4 The albedo-temperature feedback

Mote (2003) suggests that high accumulation years are often associated with low ablation for the entire ice sheet due to the well known albedo-temperature feedback. Low accumulation rates lead to more rapid losses of winter snow mass and to higher degree day factors for bare ice in the ablation zone. The higher the snow pack height at the end of spring, the later the appearance of bare ice (with a lower albedo) (Fettweis et al., 2005). A good example of the hypothesis of Mote (2003) is 1996 (see Table 2) but Fig. 11 reveals however this hypothesis does not explain the SMB variations of these last 28 years. Indeed, the winter snow accumulation has not significantly changed while the SMB variability suggests a negative trend. We have found in previous paragraphs that the thermal factors dominate currently the SMB sensitivity rather than the precipitation changes. These last results confirm our assumption.

4 The Greenland ice sheet surface energy balance

Since 1979, the SMB has been decreasing due to increasing run-off rates explained by higher temperatures. Only the increase of the long wave downward (LWD) flux and the decrease of surface albedo can explain this warming as shown in Fig. 12. No significant change occurs in both sensible and latent heat fluxes since 1979. The short wave downward (SWD) flux interannual fluctuations are very weak during the last 28 years except the negative anomalies in 1983 and 1992 due to the eruption of the El

Chichõn and the Mount Pinatubo, respectively (Hanna et al., 2005). These volcanic eruptions injected large amounts of aerosols in the atmosphere, which reduced the amount of solar energy reaching the surface of the Earth. Therefore, the net solar radiation (SWDn = SWD–[1−α]) has been increasing due to a decrease of the surface albedo (α). It is clear that an increasing melt reduces the surface albedo, which then obviously amplifies the warming-related melt increase. This amplification is particularly visible in the North-East tundra where the snow cover disappears earlier in the summers of these last years (see Fig. 7). In previous section, we have shown that the winter accumulation variability can not explain the albedo variability and Fig. 13 confirms that the albedo decrease over the 1979-2006 period starts after the middle of the summer in the tundra due to higher temperatures. Therefore, it seems reasonable to conclude that SWDn changes are rather driven by the melt increase and to a lesser extent by the rainfall increase which humidifies the snow pack and reduces the surface albedo (Fig. 8). Consequently, only the positive LWD tendency leads to the overall warming of the ice sheet surface. The net solar radiation increase is besides restricted to the ablation zone and the tundra while the infra-red radiation has been increasing everywhere as well as the 3m-temperature. The temperature is obviously better correlated with the infra-red radiation versus the solar net radiation as can be seen in Fig. 14.

5 The North Atlantic Oscillation

The North Atlantic Oscillation (NAO) represents the dominant mode of regional atmospheric variability around Greenland (e.g. Rogers, 1997; Appenzeller et al., 1998; Bromwich et al., 1999) and is gauged here by the NAO index, which is computed as the normalised pressure difference between Gibraltar minus Reykjavik (Jones et al., 1997; Osborn, 2004). It is closely related to the Arctic Oscillation (AO) (Thompson et al., 1998) and is one of the major modes of variability of the Northern Hemisphere atmosphere, particularly in winter. A large fraction of the climate changes observed during the last decades in the Arctic could besides be related to the positive trend in

the NAO/AO index during this period (e.g., Rigor et al., 2000; Moritz et al., 2003; Hanna and Cappelen, 2003; Rogers et al., 2004; Johannessen et al., 2005). The NAO is characterized by a dipole of surface pressure between mid- and high-latitudes, resulting in changes in the strength of the westerly winds in mid-latitudes and large winter temperature variations. A positive NAO phase shows a stronger than usual subtropical high pressure centre and a deeper than normal Icelandic low. The increased pressure difference results in more and stronger winter storms crossing the Atlantic Ocean on a more northerly track. This results in warm and wet winters in Europe and in cold and dry winters in northern Canada and Greenland.

According to recent observations from Johannessen et al. (2005), the maximum of the GIS sensitivity to the NAO variability is found in winter (DJF) (Table 4). The temperature (via the IR radiations) is the most sensitive component and is significantly anti-correlated to the NAO as already pointed out by Chylek et al. (2004). When the NAO indiex is negative, the location of the Icelandic low favours (southerly) warm air advection along the south west coast and over the ice sheet. This explains why the temperature correlation with the NAO is maximum in the south(west) of Greenland (Fig. 15). Everywhere and during every season, the temperature is anti-correlated to the NAO although this correlation is not significant in summer (JJA), in particular along the north-eastern coast as found by Chylek and Lohmann (2005).

Modelled precipitation variability also contains significant links with the NAO (Fig. 16). Consistent with the regional temperature sensitivity, a positive NAO phase (i.e. cold winter) is associated with less precipitation in the south east in winter (DJF) and autumn (SON). Generally, when the NAO is positive, stronger westerlies reduce the south westerly flow that brings moisture to Greenland resulting in an overall average reduction of the accumulation. Conversely, when the NAO is negative, the large-scale atmospheric flow is more frequently from the south west bringing more moisture to the ice sheet, particularly in the southern region (Mosley-Thompson et al., 2005). Except in summer (JJA), heavier precipitation is well simulated along the ice sheet eastern slope and less precipitation along the western slope during high NAO phases. This pattern

has been also identified by Appenzeller et al. (1998). Significant positive correlations with the NAO are obvious in summer (JJA) in the north west and the east.

The temperature is anti-correlated with the NAO index everywhere and in each season, and up to half of the temperature variability is explained by the NAO in winter (DJF). In summer (JJA), the sensitivity to the NAO is not significant (Table 4) in agreement with Hanna et al. (2007). Some NAO links with precipitation can also be found but they are less homogeneous in time and space. In an annual average and averaged over the ice sheet, the precipitation is not correlated with the NAO as in Hanna et al. (2006). Therefore the NAO is a good proxy for the Greenland winter temperature but does not explain the accumulation (winter snowfall) nor the melt (summer temperature) changes over the last 28 years. Beside, the last 40 years are characterized by large positive trends of NAO/AO indexes (Solomon et al., 2007) suggesting rather a cooling in Greenland and a warming in the Arctic region (Hanna and Cappelen, 2003; Goosse and Holland, 2005).

6 Discussion and conclusion

A 28-year simulation (1979–2006) of the GIS shows an insignificant increase in solid precipitation ($+0.4\pm2.5\,km^3\,yr^{-2}$) but a significant melt water production positive perturbation ($+7.9\pm3.3\,km^3\,yr^{-2}$). The increasing snowfall offsets the run-off increase to give a significant SMB mass loss rate of $-7.2\pm5.1\,km^3\,yr^{-2}$. The contribution of changes in the net water vapour fluxes to the SMB variability is negligible ($+0.02\pm0.09\,km^3\,yr^{-2}$). The melt water supply has increased because the GIS surface has been warming up by +2.4°C since 1979. More than 96% variance in the modelled surface mass balance total is explained by the summer (from 1 June to 31 August) temperature and the annual precipitation variability. A small part of the increasing liquid water supply comes from heavier rainfall ($+0.2\pm0.2\,km^3\,yr^{-2}$). Due to higher temperatures, the fraction of total precipitation that is liquid has been increasing. Snowfall shows negative trends along the ice sheet margin where the amount of liquid precipitation has been increas-

ing. The temperature has increased because of higher net solar and infra-red (IR) radiations. No significant changes in both latent and sensible heat fluxes occur. The solar power supply does not show variations during these 28 years except negative anomalies in 1983 and 1992 due to volcanic eruptions (from El Chichõn and the Mount Pinatubo). The net solar flux has increased because the albedo has been decreasing. Lower accumulation rates in winter could explain this. Indeed, low snow pack depth at the end of the winter leads to more rapid losses of winter snow mass and to higher degree day factors (i.e. higher solar radiation absorbed by the surface) for bare ice (with a lower albedo) in the ablation zone. But according to our results winter snowfall has not changed. Therefore, it is rather a result of the increasing melt which wets the snow and decreases the albedo. Besides, the net solar flux has increased only in the zone where melting has increased while the warming is occurring throughout the ice sheet. It is clear however that the decreasing albedo amplifies in turn the warming-related melt increase by the well known albedo-temperature positive feedback. Consequently, the GIS warming is mainly explained by higher incoming IR fluxes. The warming is quasi uniform over the ice sheet as the IR radiations increases, suggesting that it comes from an external forcing.

The melt has significantly increased because the GIS has been warming up at the surface in the last decades due to higher downward IR fluxes. These changes are significant and can not be explained by the natural variability (e.g. the North Atlantic Oscillation). Therefore, they could be a response (in agreement with the conclusions of Hanna et al., 2007) to the GHG concentration increase induced by the human activities since the beginning of the industrial era and its related recent global warming (Solomon et al., 2007). Higher GHG concentrations increase the incoming IR fluxes and warm up the free atmosphere. Although the MAR radiative scheme includes the interannual fluctuations of gases/aerosols concentrations, the major temporal variability comes from its boundaries via the ECMWF (re)analysis which take into account the recent GHG concentration increase and the resulting global warming. The MAR simulated 500 hPa-temperature is 0.98 correlated with the one from the (re)anlaysis which

shows an increase of $+0.07^{\circ}C\,yr^{-1}$ since 1979. Finally, the correlation between the annual MAR 3m-temperature averaged on the GIS and the global average temperature from the CRU data set (Brohan et al., 2006) is 0.66.

Since 1979, MAR simulates an increase of 102% of the freshwater flux into the ocean due to an acceleration of melt of the snow/ice at the GIS surface. This increase occurs everywhere along the Greenland coast. The maximum lies along the Greenland West coast (see Figs. 17 and 18). Integrated over the Greenland (ice sheet and tundra), the 28-year run-off rate shows a positive trend of $+8.2\pm3.5\,km^3\,yr^{-2}$ which is equivalent to a rate of global average sea level rise of $+2.3\pm1.0\times10^{-2}\,mm\,yr^{-2}$. The 28-year average of the annual Greenland run-off is $407.2\,km^3\,yr^{-1}$ (sea level equivalent is $+113\times10^{-2}\,mm\,yr^{-1}$). This flux reaches $636.8\,km^3\,yr^{-1}=2.02\times10^{-2}$ Sv in the melt record year of 2003. To this flux, we must add the glacier discharge and the basal melting flux which is normally estimated to be equal to the melt water flux. Increases in melt water suggest further an increase in glacier discharge owing to the observed melt water-induced ice sheet flow acceleration (Zwally et al., 2002). Once the ice starts to melt at the surface, it forms lakes that empty down into crevasses to the bottom of the ice. The meltwater lubricates then the motion of the glaciers.

To conclude, this paper shows that the GIS has been significantly losing mass since the beginning of eighties, by an increasing melt water run-off as well as by a probable increasing iceberg discharge into the ocean due to the effect measured by Zwally et al. (2002). The global warming induced by human activities could explain these changes. As a result, it seems that increased melting dominates over increased accumulation in a warming scenario and that the GIS will continue to loose mass in the future. The GIS melting will have an effect on the stability of the thermohaline circulation (THC) and the global sea level rise. On the one hand, increases in the freshwater flux from the GIS (glacier discharge and run-off) could perturb the THC by reducing the density contrast driving it. On the other hand, the melting of the whole GIS would account for a global mean sea level rise of 7.4 m.

Acknowledgements. All major computations were realized with the computing resources of the

Calcul Intensif et Stokage de Masse (CSIM) from the Université catholique de Louvain (http://www.cism.ucl.ac.be). The author would like to thank sincerely J.-P. van Ypersele for providing facilities while writing this paper. The comments and helps from H. Gallée, M. Erpicum, J.-P. van Ypersele, F. Lefebre, W. Lefebvre were extremely valuable.

References

Alley, R. B., Clark, P. U., Huybrechts, P., and Joughin, I.: ice sheet and sea-level changes, Science, 310, 456–460, 2005. 125

Appenzeller, C., Schwander, J., Sommer, S., and Stocker, T. F.: The North Atlantic Oscillation and its imprint on precipitation and ice accumulation in Greenland, Geophys. Res. Lett., 25(11), 1939–1942, 1998. 135, 137

Box, J. E. and Steffen, K.: Sublimation estimates for the Greenland ice sheet using automated weather station observations, J. Geophys. Res., 106(D24), 33 965–33 982, 2001. 125, 129

Box, J. E. and Rinke, A.: Evaluation of Greenland ice sheet surface climate in the HIRHAM regional climate model, J. Clim., 16, 1302–1319, 2003. 126

Box, J. E., Bromwich, D. H., and Bai, L.-S.:Greenland ice sheet surface mass balance for 1991–2000: application of Polar MM5 mesoscale model and in-situ data, J. Geophys. Res., 109(D16), D16105, doi:10.1029/2003JD004451, 2004. 125, 128, 130, 132

Box, J. E., Bromwich, D. H., Veenhuis, B. A., Bai, L.-S., Stroeve, J. C., Rogers, J. C., Steffen, K., Haran, T., and Wang, S.-H.: Greenland ice sheet surface mass balance variability (1988–2004) from calibrated Polar MM5 output, J. Climate, 19(12), 2783–2800, 2006. 126, 127, 128, 129, 130, 131, 147

Box, J. E. and Cohen, A. E.: Upper-air temperatures around Greenland: 1964–2005, Geophys. Res. Lett., 33, L12706, doi:10.1029/2006GL025723, 2006. 127

Brohan, P., Kennedy, J. J., Haris, I., Tett, S. F. B., and Jones, P. D.: Uncertainty estimates in regional and global observed temperature changes: a new dataset from 1850, J. Geophys. Res., 111, D12106, doi:10.1029/2005JD006548, 2006. 139

Bromwich, D. H., Chen, Q. S., Li, Y. F., and Cullather, R. I.: Precipitation over Greenland and its relation to the North Atlantic Oscillation, J. Geophys. Res., 104(D18), 22 103–22 115, 1999. 135

Brun, E., David, P., Sudul, M., and Brunot, G.: A numerical model to simulate snowcover stratigraphy for operational avalanche forecasting, J. Glaciol., 38, 13–22, 1992. 128
Bugnion, V. and Stone, P. H.: Snowpack model estimates of the mass balance of the Greenland ice sheet and its changes over the twenty first century, Clim. Dyn., 20, 87–106, 2002. 130, 147
Chen J. L., Wilson, C. R., and Tapley, B. D.: Satellite Gravity Measurements Confirm Accelerated Melting of Greenland Ice Sheet, Science, 313, 1958–1960, doi:10.1126/science.1129007, 2006. 126, 131
Chylek, P., Box, J. E., and Lesins, G.: Global Warming and the Greenland Ice Sheet, Climatic Change, 63, 201–221, 2004. 136
Chylek, P. and Lohmann, U.: Ratio of the Greenland to global temperature change: Comparison of observations and climate modeling results, Geophys. Res. Lett., 32, L14705, doi:10.1029/2005GL023552, 2005. 136
Chylek, P., Dubey, M. K., and Lesins, G.: Greenland warming of 1920-1930 and 1995–2005, Geophys. Res. Lett., 33, L11707, doi:10.1029/2006GL026510, 2006. 127
Cogley, J. G.: Greenland accumulation: An error model, J. Geophys. Res., 109, D18101, doi:10.1029/2003JD004449, 2004. 129
De Ridder, K. and Gallée, H.: Land surface-induced regional climate change in Southern Israel, J. Appl. Meteorol., 37, 1470–1485, 1998. 127
Dethloff, K., Schwager, M., Christensen, J. H., Kiilsholm, S., Rinke, A., Dorn, W., Jung-Rothenhäusler, F., Fischer, H., Kipfstuhl, S., and Miller, H.: Recent Greenland accumulation estimated from regional model simulations and ice core ananlysis, J. Clim., 15, 2821–2832, 2002. 126
Dowdeswell, J.: The Greenland Ice Sheet and Global Sea-Level Rise, Science 17 February 2006, 311(5763), 963–964, doi:10.1126/science.1124190, 2006. 125
Fettweis, X., Gallée, H., Lefebre, L., and van Ypersele, J.-P.: Greenland surface mass balance simulated by a regional climate model and comparison with satellite derived data in 1990–1991, Clim. Dyn., 24, 623–640, doi:10.1007/s00382-005-0010-y, 2005. 127, 128, 129, 130, 134
Fettweis, X., Gallée, H., Lefebre, L., and van Ypersele, J.-P.: The 1988–2003 Greenland ice sheet melt extent by passive microwave satellite data and a regional climate model, Clim. Dyn., 27(5), 531–541, doi:10.1007/s00382-006-0150-8, 2006. 126, 127
Fettweis, X., van Ypersele, J.-P., Gallée, H., Lefebre, F., and Lefebvre, W.: The 1979-

2005 Greenland ice sheet melt extent from passive microwave data using an improved version of the melt retrieval XPGR algorithm, Geophys. Res. Lett., 34, L05502, doi:10.1029/2006GL028787, 2007. 126, 127

Gallée, H. and Schayes, G.: Development of a three-dimensional meso-γ primitive equations model, Mon. Wea. Rev., 122, 671–685, 1994. 127

Gallée, H., Guyomarc'h, G. and Brun, E.: Impact of the snow drift on the Antarctic ice sheet surface mass balance: possible sensitivity to snow-surface properties, Boundary-Layer Meteorol., 99, 1–19, 2001. 128

Goosse, H. and Holland, M.: Mechanisms of decadal Arctic variability in the Community Climate System Model CCSM2, J. Climate, 18(17), 3552–3570, 2005. 137

Greuell, W., Denby, B., van de Wal, R. S. W., and Oerlemans, J.: Ten years of massbalance measurements along a transect near Kangerlussuaq, Greenland, J. Glaciol., 47, 157–158, 2001. 126, 132

Hanna, E., Huybrechts, P., and Mote, T.: Surface mass balance of the Greenland ice sheet from climate analysis data and accumulation/run-off models, Ann. Glaciol., 35, 67–72, 2002. 126, 129

Hanna, E. and Cappelen, J.: Recent cooling in coastal southern Greenland and relation with the North Atlantic Oscillation, Geophys. Res. Lett., 30, 1132, doi:10.1029/2002GL015797, 2003. 136, 137

Hanna, E., Huybrechts, P., Janssens, I., Cappelen, J., Steffen, K., and Stephens, A.: Runoff and mass balance of the Greenland ice sheet: 1958–2003, J. Geophys. Res., 110, D13108, doi:10.1029/2004JD005641, 2005. 126, 130, 135, 147

Hanna, E., McConnell, J., Das, S., Cappelen, J., and Stephens, A.: Observed and modeled Greenland ice sheet snow accumulation, 1958–2003, and links with regional climate forcing, J. Climate, 19, 344–358, 2006. 129, 137

Hanna, E., Huybrechts, P., Steffen, K., Cappelen, J., Huff, R., Shuman, C., Irvine-Fynn, T., Wise, S. and Griffiths, M.: Increased runoff from melt from the Greenland Ice Sheet: a response to global warming, J. Climate, accepted, 2007. 130, 137, 138

Howat, I. M., Joughin, I. Tulaczyk,, S., and Gogineni, S.: Rapid retreat and acceleration of Helheim Glacier, east Greenland, Geophys. Res. Lett., 32, L22502, doi:10.1029/2005GL024737, 2005. 125

Howat, I. M., Joughin, I. and Scambos, T. A.: Rapid Changes in Ice Discharge from Greenland Outlet Glaciers, Science, 315(5818), 1559, doi:10.1126/science.1138478, 2007. 126

Janssens, I. and Huybrechts, P.: The treatment of meltwater retention in mass-balance parameterizations of the Greenland ice sheet, Ann. Glaciol., 31, 133–140, 2000. 147

Johannessen, O. M., Khvorostovsky, K., Miles, M. W., and Bobylev, L. P.: Recent ice sheet growth in the interior of Greenland, Sciencexpress, 20 October 2005, 1013–1016, doi:10.1126/science.1115356, 2005. 126, 131, 136, 149

Jones, P. D., Jonsson, T., and Wheeler, D.: Extension to the North Atlantic Oscillation using early instrumental pressure observations from Gibraltar and South-West Iceland, Int. J. Climatol. 17, 1433–1450, 1997. 135

Krabill, W., Frederick, E., Manizade, S., Martin, C., Sonntag, J., Swift, R. Thomas,, R., Wright, W., and Yngel, J.: Rapid thinning of parts of the southern Greenland ice sheet, Science, 283, 1522–1524, 1999. 125, 126

Krabill, W., Abdalati, W., Frederick, E., Manizade, S., Martin, C., Sonntag, J., Swift, R., Thomas, R., Wright, W., and J. Yungel: Greenland Ice Sheet: High-Elevation Balance and Peripheral Thinning, Science, 289, 428–430, 2000. 126

Krabill, W., Hanna, E., Huybrechts, P., Abdalati, W., Cappelen, J., Csatho, B., Frederick, E., Manizade, S., Martin, C., Sonntag, J., Swift, R., Thomas, R., and Yungel, J.: Greenland Ice Sheet: Increased coastal thinning, Geophys. Res. Lett., 31, L24402, doi:10.1029/2004GL021533, 2004. 126

Lefebre, F., Gallée, H., van Ypersele, J., and Greuell, W.: Modeling of snow and ice melt at ETH-camp (west Greenland): a study of surface albedo, J. Geophys. Res., 108(D8), 4231, doi:10.1029/2001JD001160, 2003. 127, 156

Lefebre, F., Fettweis, X., Gallée, H., van Ypersele, J., Marbaix, P., Greuell, W., and Calanca, P.: Evaluation of a high-resolution regional climate simulation over Greenland, Clim. Dyn., 25, 99–116, doi:10.1007/s00382-005-0005-8, 2005. 127, 128

Lemke, P., Ren, J., Alley, R. B., Allison, I., Carrasco, J., Flato, G., Fujii, Y., Kaser, G., Mote, P., Thomas, R. H., and Zhang, T.: Observations: Changes in Snow, Ice and Frozen Ground. In: Climate Change 2007: The Physical Science Basis. Contribution of Working Group I to the Fourth Assessment Report of the Intergovernmental Panel on Climate Change, edited by: Solomon, S., Qin, D., Manning, M., Chen, Z., Marquis, M., Averyt, K. B., Tignor, M., and Miller, H. L., Cambridge University Press, Cambridge, United Kingdom and New York, NY, USA, 2007. 125, 126

Luckman, A. and Murray, T.: Seasonal variation in velocity before retreat of Jakobshavn Isbr, Greenland, Geophys. Res. Lett., 32, L08501, doi:10.1029/2005GL022519, 2005. 125

Luckman, A., Murray, T., de Lange, R., and Hanna, E.: Rapid and synchronous ice-dynamic changes in East Greenland, Geophys. Res. Lett., 33, L03503, doi:10.1029/2005GL025428, 2006. 125

Luthcke, S. B., Zwally, H. J., Abdalati, W., Rowlands, D. D., Ray, R. D., Nerem, R. S., Lemoine, F. G., McCarthy, J. J., and Chinn, D. S.: Recent Greenland Ice Mass Loss by Drainage System from Satellite Gravity Observations, Science, 314(5803), 1286, doi:10.1126/science.1130776, 2006 126, 131

Mosley-Thompson, E., Readinger, C. R., Craigmile, P., Thompson, L. G., and Calder, C. A.: Regional sensitivity of Greenland precipitation to NAO variability, Geophys. Res. Lett., 32, L24707, doi:10.1029/2005GL024776, 2005. 136

Moritz, R. E., Bitz, C. M., and Steig, E. J.: Dynamics of recent climate change in the Arctic, Sciences, 297, 1497–1502, 2003. 136

Mote, T. L.: Estimation of runoff rates, mass balance, and elevation changes on the Greenland ice sheet from passive microwave observations, J. Geophys. Res., 108(D2), 4056, doi:10.1029/2001JD002032, 2003. 126, 130, 134, 147

Ohmura, A., Calanca, P., Wild, M., and Anklin, M.: Precipitation, accumulation, and mass balance of the Greenland ice sheet, Zeit. Gletsch. Glazialgeol, 35, 1–20, 1999. 129

Osborn, T. J.: Simulating the winter North Atlantic Oscillation: the roles of internal variability and greenhouse gas forcing, Clim. Dyn., 22, 605–623, 2004. 135

Rahmstorf, S., Crucifix, M., Ganopolski, A., Goosse, H., Kamenkovich, I., Knutti, R., Lohmann, G., Marsh, R., Mysak, L. A., Wang, Z., and Weaver, A. J.: Thermohaline circulation hysteresis: A model intercomparison, Geophys. Res. Lett., 32(23), L23605, doi:10.1029/2005GL023655, 2005. 125

Reeh, N., Mayer, C., Miller, H., Thomson, H. H., and Weidick, A.: Present and past climate control on fjord glaciations in Greenland: Implications for IRD-deposition in the sea, Geophys. Res. Lett., 26, 1039–1042, 1999. 125, 129, 147

Ridley, J., Huybrechts, P., Gregory, J., and Lowe, J.: Future changes in the Greenland ice sheet: A 3000 year simulation with a high resolution ice sheet model interactively coupled to an AOGCM, J. Climate, 18, 3409–3427, 2005. 125

Rignot, E., Braaten, D., Gogineni, S. P., Krabill, W. B., and McConnell, J. R.: Rapid ice discharge from southeast Greenland glaciers, Geophys. Res. Lett., 31, L10401, doi:10.1029/2004GL019474, 2004. 126

Rignot, E. and Kanagaratnam, P.: Changes in the Velocity Structure of the Greenland Ice

Sheet, Science 17 February 2006, 311, 986–990, doi:10.1126/science.112138, 2006. 125, 126
Rigor, I. G., Wallace, J. M., and Colony, R. L.: Response of sea ice to the Arctic Oscillation, J. Climate, 15, 2648–2663, 2000. 136
Rogers, J. C.: North Atlantic storm track variability and its association to the North Atlantic Oscillation and climate variability of Northern Europe, J. Climate, 10(7), 1635–1647, 1997. 135
Rogers, J. C., Wang, S. H., and Bromwich, D. H.: On the role of the NAO in recent northeastern Atlantic Arctic warming, Geophys. Res. Lett., 31, L02201, doi:10.1029/2003GL018728, 2004. 136
Snedecor, G. W. and Cochran, W. G.: Méthodes statistiques, Original Title: Statistical Methods 6th edition by The Iowa State University Press, Ames, Iowa, USA, 67-21577, traduit par H. Boelle et E. Camhaji, Association de Coordination Technique Agricole, Paris, 649 pp, 1971. 131
Solomon, S., Qin, D., Manning, M., Alley, R. B., Berntsen, T., Bindoff, N. L., Chen, Z. Chidthaisong,, A., Gregory, J. M., Hegerl, G. C., Heimann, M., Hewitson, B., Hoskins, B. J., Joos, F., Jouzel, J., Kattsov, V,. Lohmann, U., Matsuno, T., Molina, M., Nicholls, N., Overpeck, J., Raga, G., Ramaswamy, V., Ren, J., Rusticucci, M., Somerville, R., Stocker, T. F., Whetton, P., Wood, R. A., and Wratt, D.: Technical Summary in: Climate Change 2007: The Physical Science Basis. Contribution of Working Group I to the Fourth Assessment Report of the Intergovernmental Panel on Climate Change, edited by: Solomon, S., Qin, D., Manning, M., Chen, Z., Marquis, M., Averyt, K. B., Tignor, M., and Miller , H. L., Cambridge University Press, Cambridge, United Kingdom and New York, NY, USA, 2007. 124, 125, 137, 138
Thomas, R., Csatho, B., Davis, C., Kim, C., Krabill, W., Manizade, S., McConnell, J., and Sonntag, J.: Mass balance of higher-elevation parts of the Greenland ice sheet, J. Geophys. Res., 106(D24), 33 707, doi:10.1029/2001JD900033, 2001. 126
Thomas, R., Frederick, E., Krabill, W., Manizade, S., and Martin, C.: Progressive increase in ice loss from Greenland, Geophys. Res. Lett., 33, L10503, doi:10.1029/2006GL026075, 2006. 126, 131, 149
Thompson, D. W. J. and Wallace, J. M.: The Arctic Oscillation signature in the wintertime geopotential height and temperature fields, Geophys. Res. Lett., (9), 1297–1300, 1998. 135
Velicogna, I., and Wahr, J.: Greenland mass balance from GRACE, Geophys. Res. Lett., 32, L18505, doi:10.1029/2005GL023955, 2005. 126, 131

Zwally, J. H. and Giovinetto, M. B.: Balance mass flux and ice velocity across the equilibrium line in drainage systems of Greenland, J. Geophys. Res., 106, 33 717–33 728, 2001. 125, 130, 133, 160

Zwally, J. H., Abdalati, W., Herring, T., Larson, K., Saba, J., and Steffen, K.: Surface Melt-Induced Acceleration of Greenland Ice-Sheet Flow, Science, 297, 218–222, 2002. 125, 129, 132, 139

Zwally, J. H., Giovinetto, M., Li,J., Cornejo,H., Beckley, M., Brenner, A., Saba, J., and Yi, D.: Mass changes of the Greenland and Antarctic ice sheets and shelves and contributions to sea-level rise: 1992–2002, J. Glaciol., 51(175), December 2005, 509–527(19), 2005. 126, 131, 149

Table 1. Annual mass balance components simulated by MAR, Polar MM5 (Box et al., 2006), ECHAM4 and MIT models (Bugnion and Stone, 2002), a PDD model (Janssens and Huybrechts, 2000), derived from the ECMWF (re)analysis (Hanna et al., 2005), derived from SSM/I observations (Mote, 2003) and estimated by Reeh et al. (1999) which use in situ observations. The period over which it is averaged and the ice sheet area is also shown. Accumulation is calculated as snowfall plus rainfall minus erosion from the net water fluxes and the wind (blowing snow). Units are $km^3\ yr^{-1}$.

Model	Period	Area ($\times 10^6$ km^2)	Snowfall	Rainfall	Subli. / Evap.	Blowing snow	Accumulation	Runoff	Surface mass balance	Iceberg calving	Basal melting
MAR	1979–2005	1701	594±53	24±5	5±2		612±55	304±96	**308±125**		
Polar MM5	1988–2004	1691	617±59	24±7	64±8	34±6	543±131	373±66	**170±152**		
ECHAM4	1990's		585		46		540	122			
MIT	1990's		649		95		554	162			
PDD model	1990's	1,691					542	281	**262±39**		
ECMWF analysis	1958–2003						573±70	280±69	**293±104**		
Mote (2003)	1988–1999	1,648	620	25	75		539	278	**261**		
Reeh et al. (1999)	1990's	1,707					602	304	**298**	263	35

Table 2. Annual surface mass balance components (Units are $km^3\ yr^{-1}$) and annual temperature anomaly (Units are $°C\ yr^{-1}$).

	Snowfall	Rainfall	Subli./Evap.	Runoff	SMB	Temp. Ano.
1979	592.2	18.7	3.0	202.7	405.2	–0.3
1980	592.8	17.8	7.1	276.4	327.1	0.4
1981	572.6	27.6	6.2	281.7	312.3	–0.8
1982	532.6	17.0	6.1	255.1	288.4	–1.0
1983	638.3	24.5	2.8	131.7	528.3	–2.2
1984	648.0	27.7	3.4	226.1	446.1	–1.2
1985	490.3	19.1	9.1	335.6	164.7	0.6
1986	612.0	18.7	5.7	200.3	424.8	–0.5
1987	577.9	18.9	3.2	311.9	281.8	0.4
1988	564.5	23.8	6.6	277.4	304.3	–0.1
1989	532.6	27.8	6.2	300.9	253.4	–1.4
1990	589.1	25.3	6.7	316.5	291.2	–0.7
1991	618.8	22.5	4.2	311.6	325.5	–0.5
1992	640.7	14.9	1.5	99.3	554.7	–1.9
1993	584.6	24.0	5.9	264.6	338.1	–1.3
1994	571.5	21.7	6.1	229.6	357.6	–0.8
1995	582.3	22.1	6.0	317.9	280.6	0.3
1996	730.0	24.9	3.1	194.3	557.6	1.1
1997	662.7	24.2	5.0	295.1	386.9	0.7
1998	560.7	24.8	6.5	427.3	151.7	1.3
1999	638.6	24.6	1.5	320.3	341.4	0.0
2000	617.9	37.6	2.6	364.6	288.2	0.6
2001	660.4	23.8	3.8	372.1	308.2	1.2
2002	552.0	27.0	9.0	410.9	159.1	1.3
2003	601.7	33.4	7.5	526.9	100.7	1.3
2004	579.4	28.3	5.8	442.9	159.0	0.9
2005	607.1	21.5	7.5	408.3	212.8	1.6
2006	472.7	26.1	4.7	409.7	84.4	1.0
Mean	593.7	23.9	5.2	304.0	308.4	0.0
Min	472.7	14.9	1.5	99.3	84.4	–2.2
Max	730.0	37.6	9.1	526.9	557.6	1.6
Range	53.4	4.9	2.1	96.2	125.0	1.1
Trend	0.4	0.3	0.0	7.9	–7.2	0.1

Table 3. Rates of surface elevation change (dS/dt) simulated by the MAR model, derived from ERS satellite radar altimeter data (Johannessen et al., 2005; Zwally et al., 2005) and, from the NASA's airborne (Airborne Topographic Mapper, ATM) and the satellite (ICEsat) laser altimeter surveys (Thomas et al., 2006). The period over which it is averaged is shown. Units are mm yr^{-1}.

Data	Period	<1500 m	≥1500 m	< 2000 m	≥ 2000 m	Total
MAR model	1979–2006	–29±16	–15±27	–40±24	–4±20	–9±8
MAR model	1992–2003	–103±80	–44±120	–137±99	–10±83	–29±34
ERS data (Johannessen et al., 2005)	1992–2003	–20±9	+64±5	+25±7	+65±4	+54±2
ERS data (Zwally et al., 2005)	1992–2002	–56±14	+42±5	–14±12	+48±2	+27±3
ATM/ICEsat data (Thomas et al., 2006)	1993–2004	–257±30	+12±10	–153±17	+24±10	–45±11

Table 4. Mean Greenland ice sheet sensitivity to the NAO for the 1979–2006 period. The North Atlantic Oscillation (NAO) index comes from the Climate Research Unit (CRU) available at http://www.cru.uea.ac.uk/cru/data/nao.htm.

	Winter (DJF)	Spring (MAM)	Summer (JJA)	Autumn (SON)	Year
Precipitation	–0.42	–0.32	0.18	–0.33	–0.13
3m-Temperature	–0.76	–0.45	–0.23	–0.56	–0.67

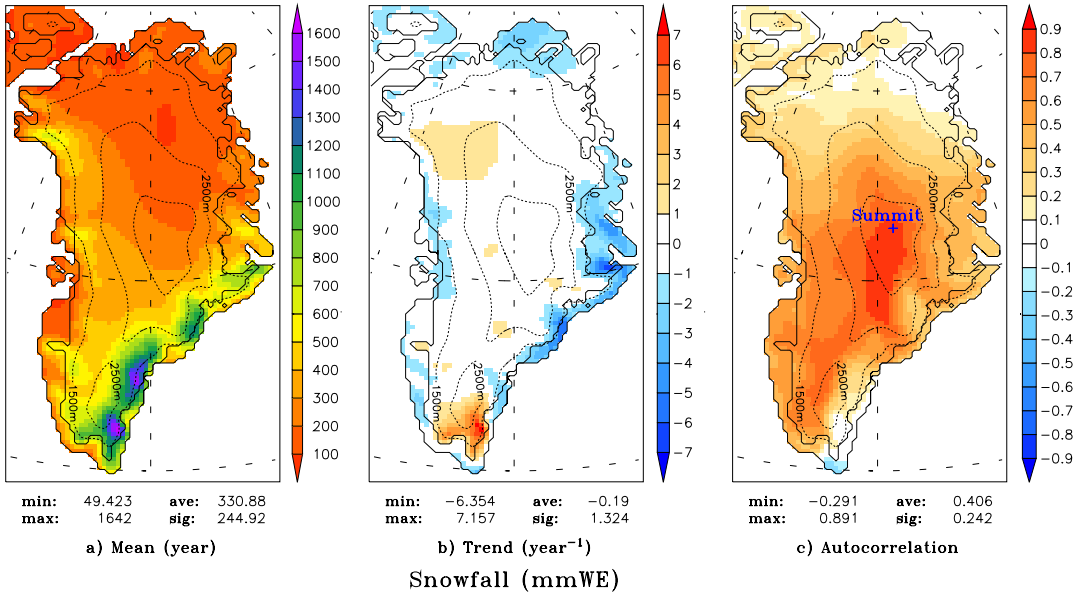

Fig. 1. The 1979–2006 annual mean (left), 28-year linear regression change (centre) and autocorrelation (right) of the snowfall. The autocorrelation is defined as the correlation between time series of the annual total ice sheet snowfall with that at each grid location. Units are mm of water equivalent (mmWE). The autocorrelation shows where regional variability best captures the variability over the complete ice sheet. Finally, minimum and maximum values are indicated as well as the ice sheet average and the standard deviation.

TCD
1, 123–168, 2007

EGU

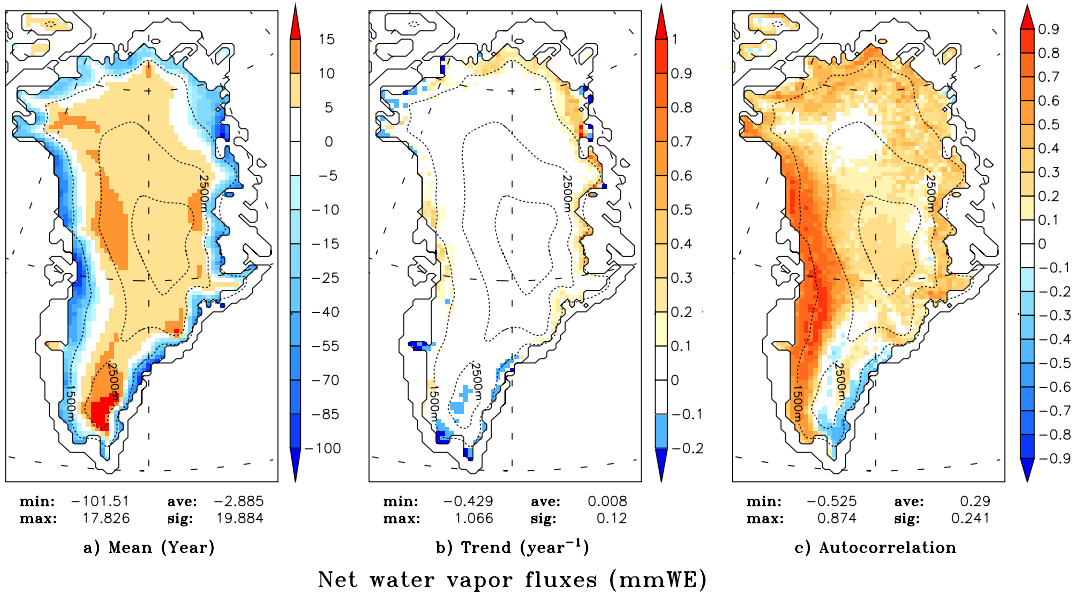

Fig. 2. Same as Fig. 1 but for the net surface water vapour fluxes (i.e. the evaporation, condensation, sublimation and deposition).

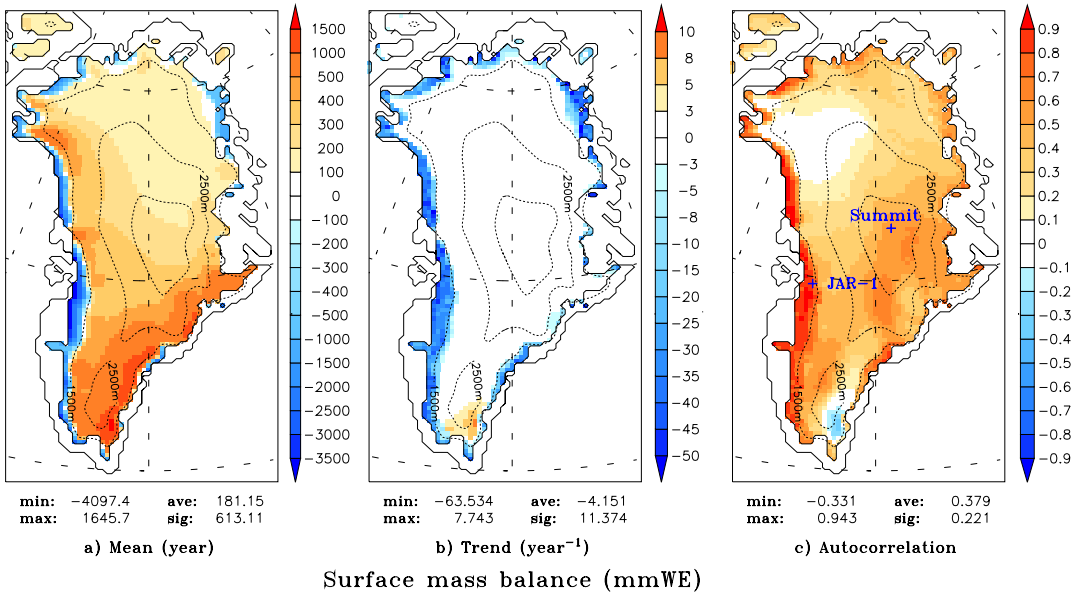

Fig. 3. Same as Fig. 1 but for the SMB. The plot **(a)** shows the mean accumulation zone in red and the ablation zone in blue. The equilibrium zone, where the average SMB over the last 28 years is null, is plotted in white. The plot **(c)** shows that the melt variability in the (western) ablation zone is more important than the solid precipitation variability to influence the SMB.

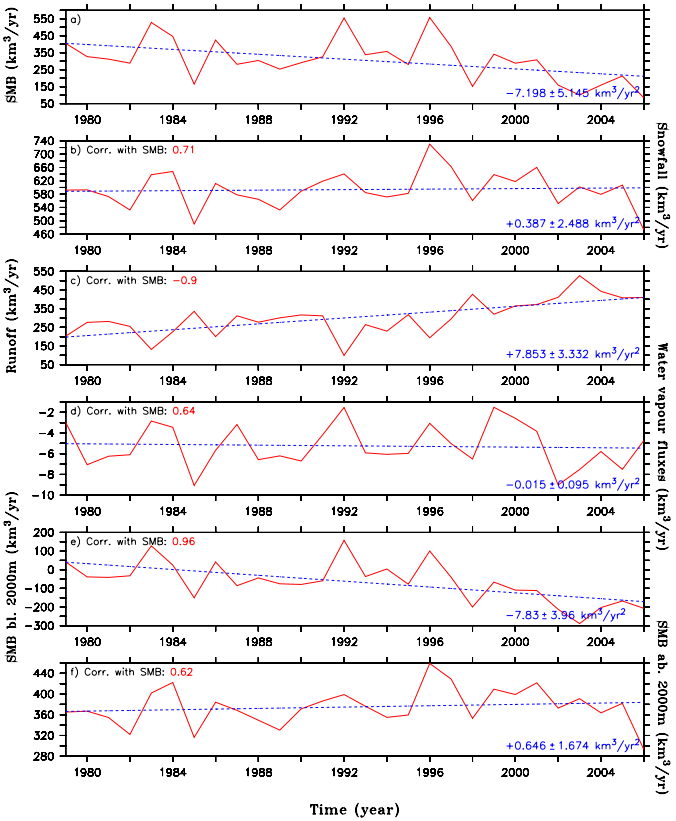

Fig. 4. Time series of the annual total ice sheet **(a)** SMB, **(b)** snowfall, **(c)** run-off, **(d)** net water vapour fluxes, **(e)** SMB averaged over the ice sheet area below 2000 m and **(f)** above 2000 m. Units are $km^3\ yr^{-1}$. The correlation with the whole ice sheet SMB is indicated as well as the trend. The linear trends are in $km^3\ yr^{-2}$.

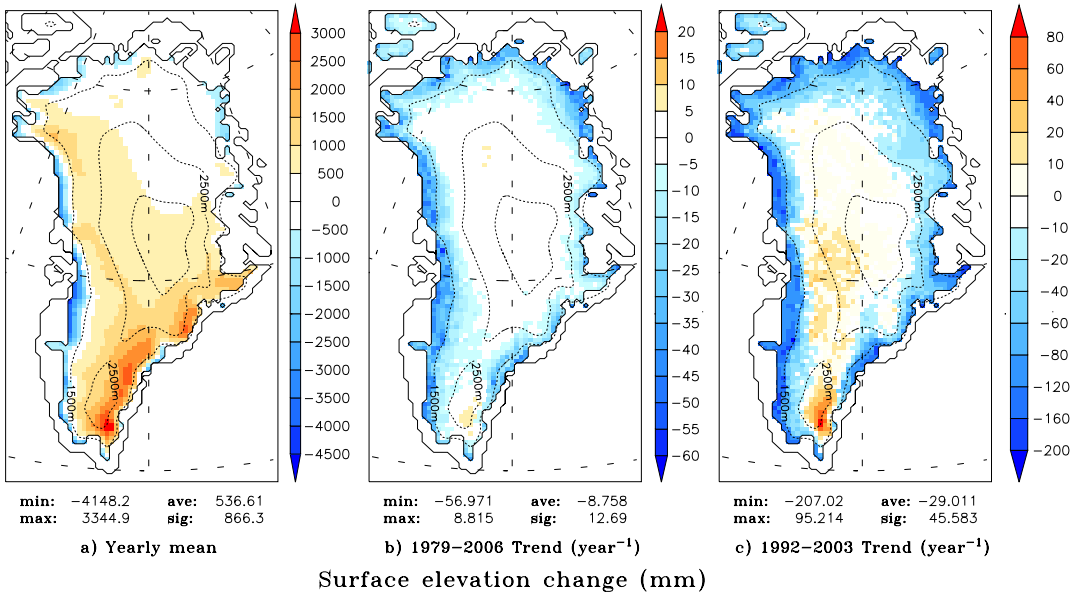

Fig. 5. Rates of elevation change (dS/dt) in cm yr^{-1} for the 1992–2003 period and the 1979–2006 period. Only the changes due to the interannual variability of the snowfall, melt and water vapour fluxes are taken into account here. The topography (and consequently the margin glaciers) of the ice sheet is assumed to be constant during the simulation.

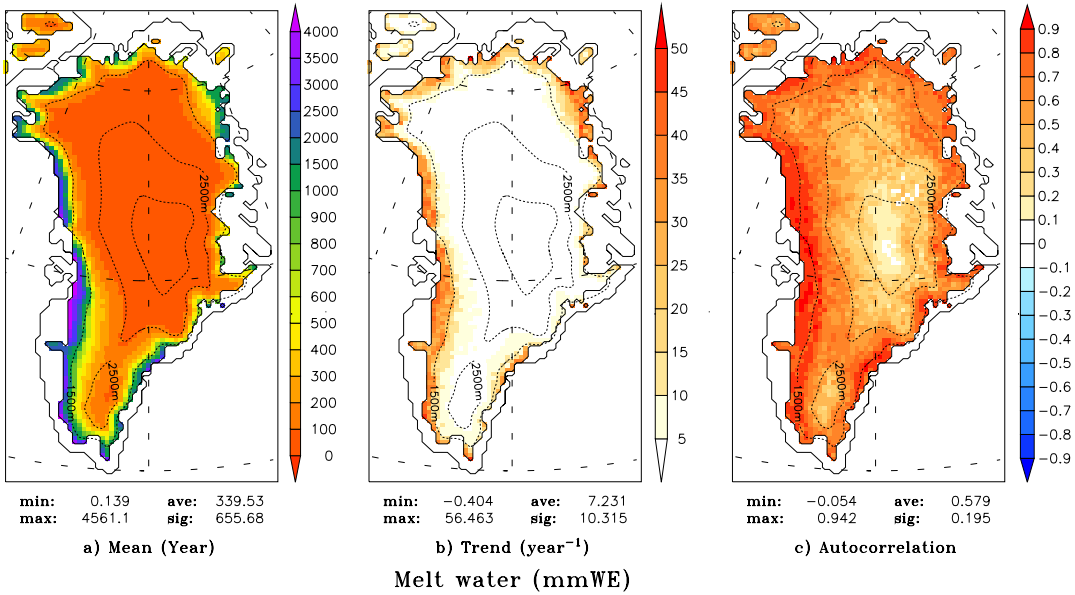

Fig. 6. Same as Fig. 1 but for available melt water. Part of this meltwater is refrozen and does not reach the ocean (Lefebre et al., 2003).

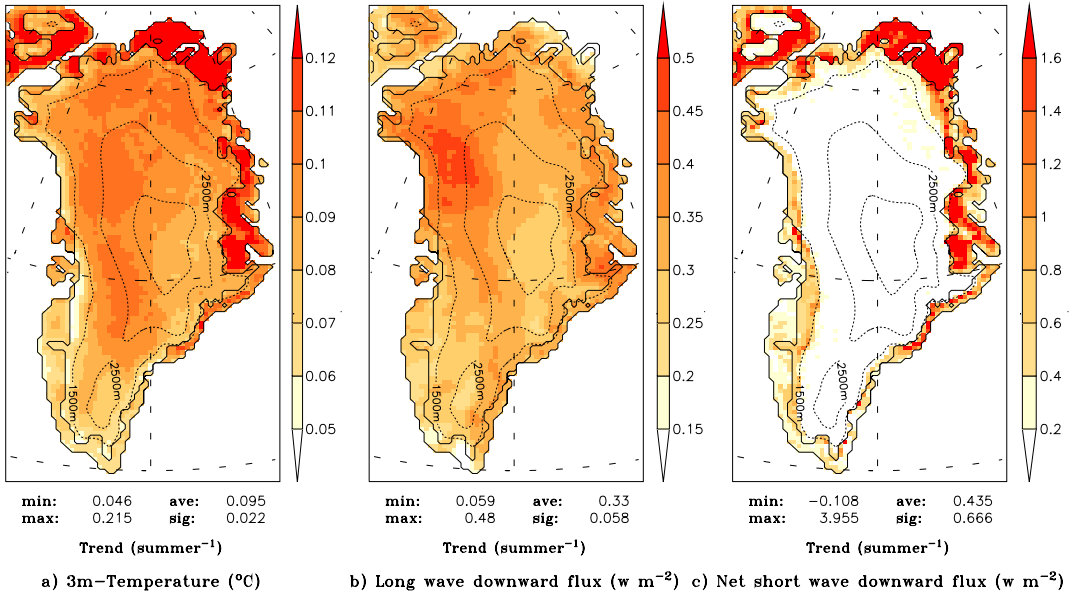

Fig. 7. The 28-year linear regression change for the summer 3m-Temperature (left), for the summer downward infra-red radiation (centre) and for the summer solar net radiation (right).

TCD
1, 123–168, 2007

EGU

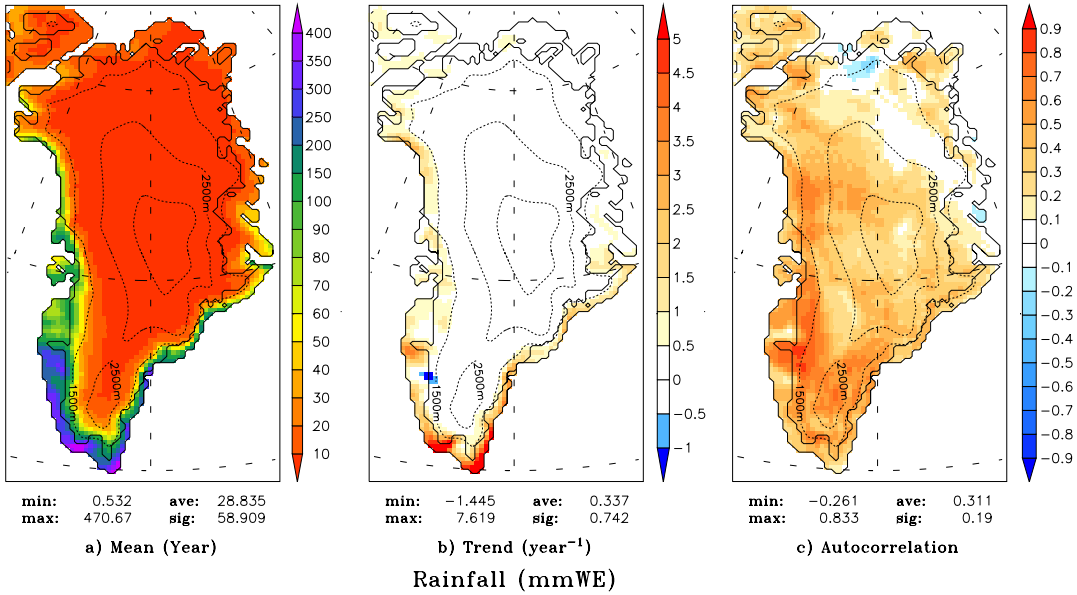

Fig. 8. Same as Fig. 1 but for rainfall.

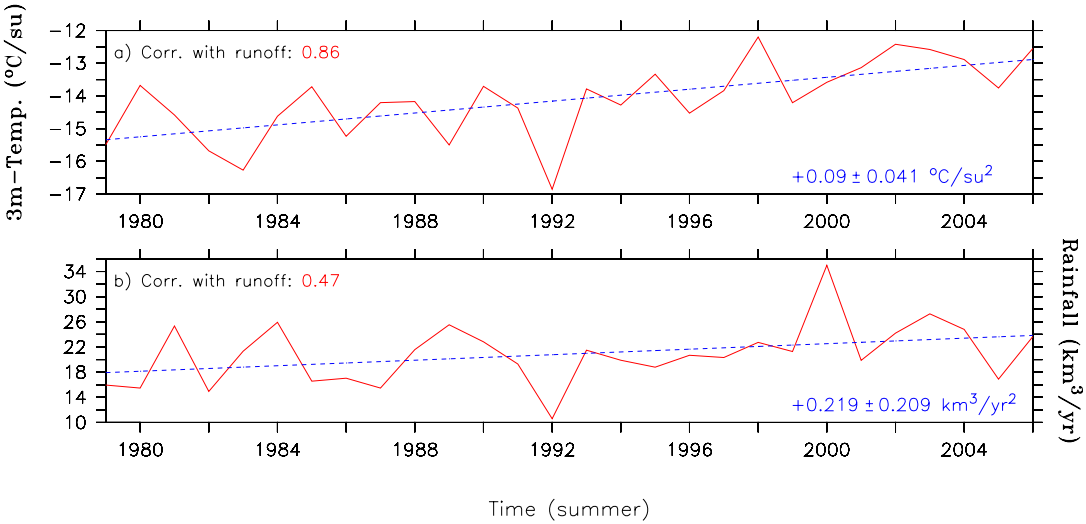

Fig. 9. Time series of the total ice sheet **(a)** summer (from 1 May to 30 September) temperature average (in ˚C su-1) and **(b)** yearly rainfall (in km^3 yr^{-1}). The correlation with the run-off (Fig. 4) is indicated as well as the trend.

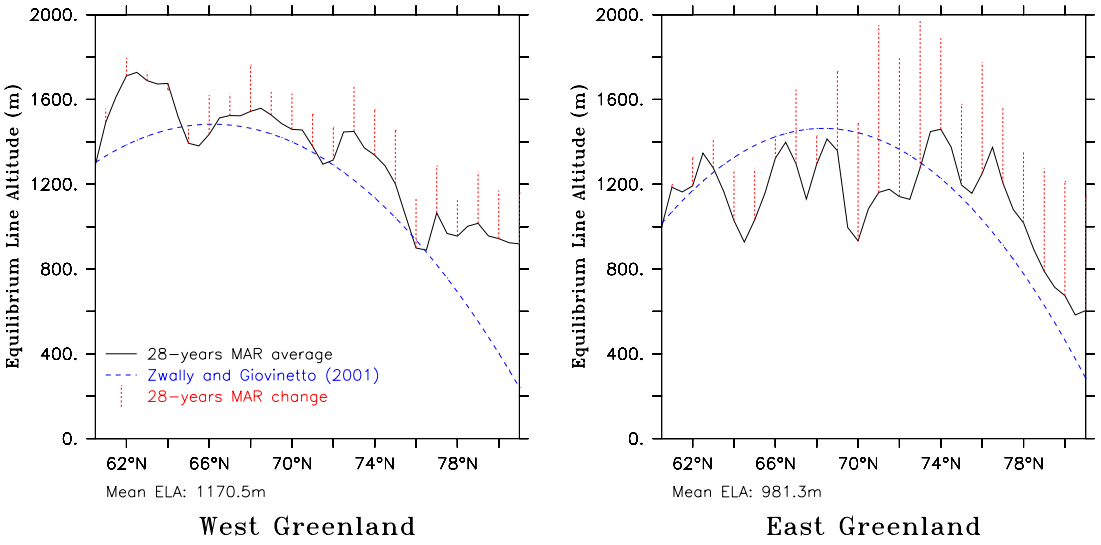

Fig. 10. Average equilibrium line altitude variations in MAR simulation (solid) and estimated by Zwally and Giovinetto (2001) parametrization (dashed). The MAR 28-year changes are also shown (dotted).

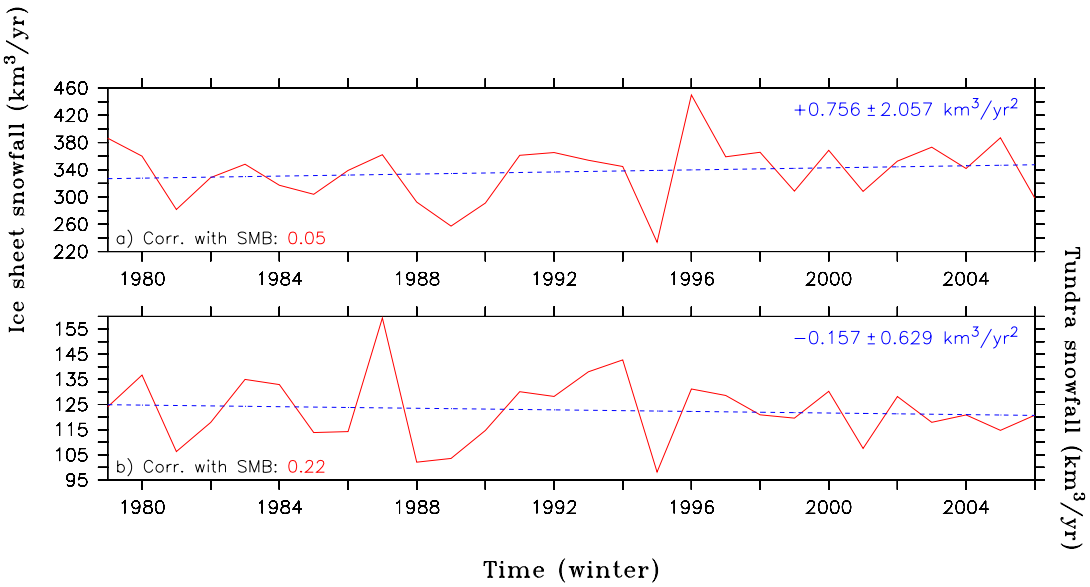

Fig. 11. Time series of the winter (from 1 October YEAR-1 to 30 April YEAR) snowfall before the considered year (in km^3 yr^{-1}) over **(a)** the ice sheet and **(b)** the tundra. The correlation with the SMB (Fig. 4) is indicated.

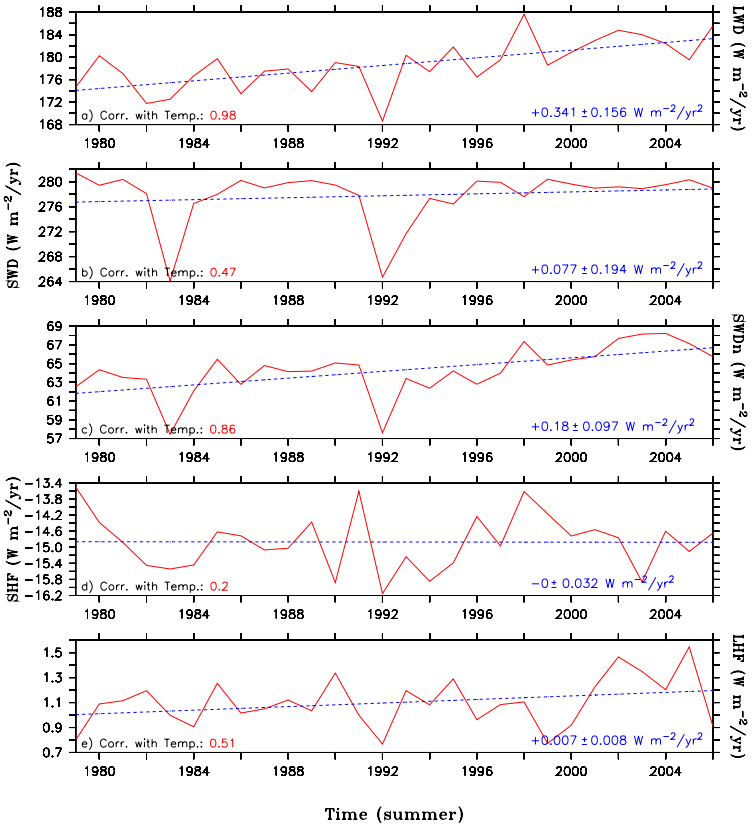

Fig. 12. Time series of the mean summer total ice sheet **(a)** long wave downward flux (LWD), **(b)** short wave downward flux (SWD), **(c)** net short wave downward flux (SWDn), **(d)** sensible heat flux (SHF) and **(e)** latent heat flux (LHF). The correlation with the 3 m-temperature (see Fig. 9) is indicated. Units are in W/m^2.

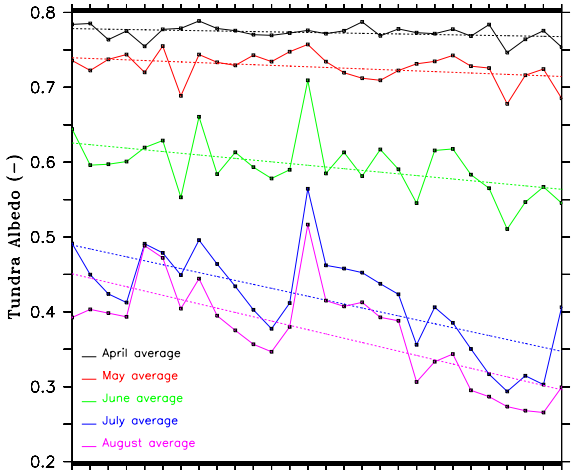

Fig. 13. Time series of the averaged tundra albedo for April, May, June, July and August. The 1979–2006 linear trend is dashed.

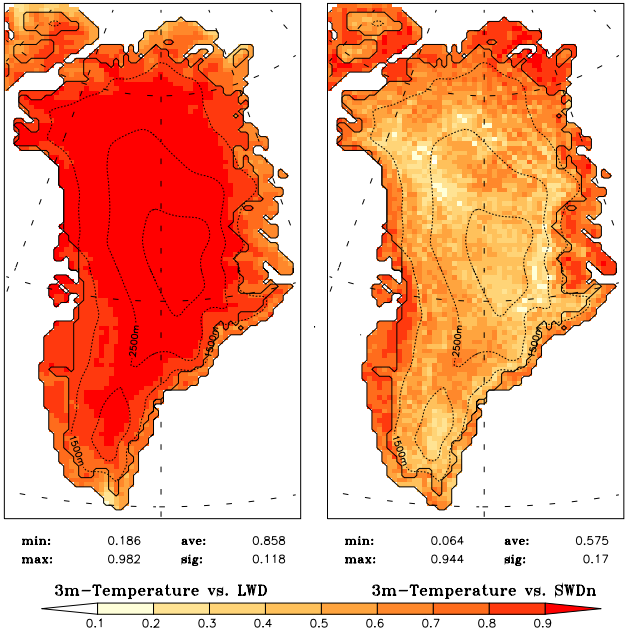

Fig. 14. Correlation coefficient between the 3 m-temperature and the infra-red radiation (left) and the net solar radiation (right) in summer, respectively. The correlation coefficient is computed by using the annual time series of each pixel.

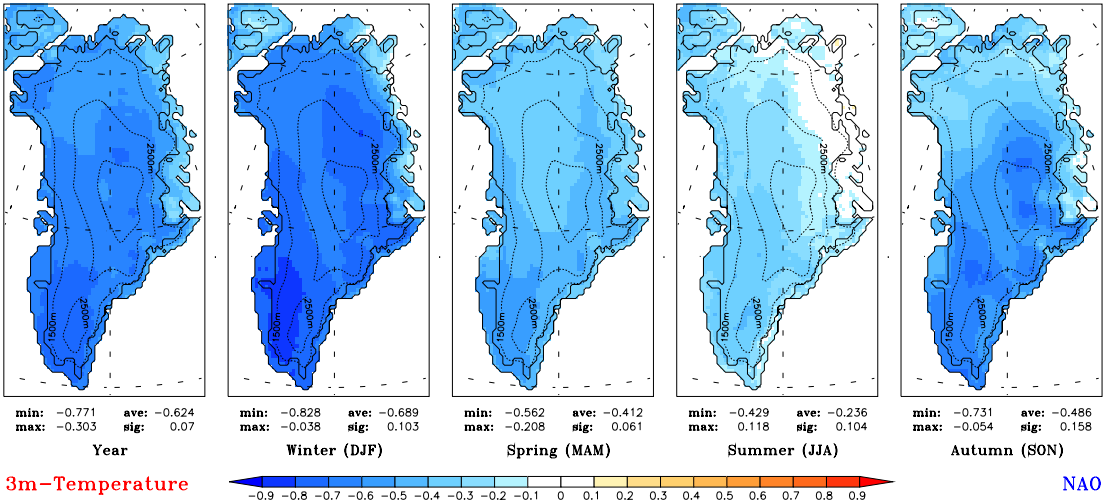

Fig. 15. Greenland ice sheet seasonal temperature sensitivity to the NAO. Only correlation coefficients above 0.3 are significant. The maps going from left to right are respectively the annual, winter (DJF), spring (MAM), summer (JJA) and autumn (SON) mean. The North Atlantic Oscillation (NAO) index comes from the Climate Research Unit (CRU) available at http://www.cru.uea.ac.uk/cru/data/nao.htm.

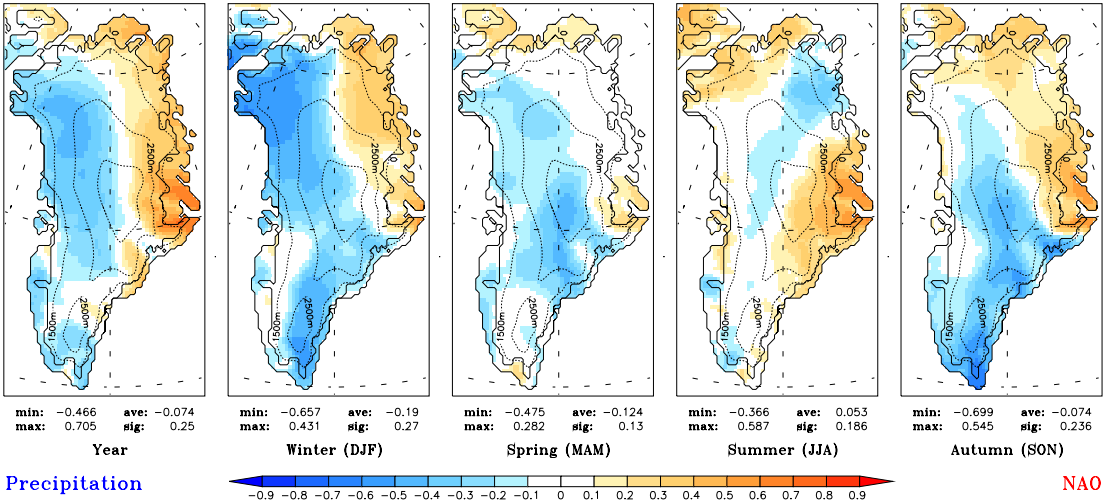

Fig. 16. Same as Fig. 15 but for precipitation (solid and liquid).

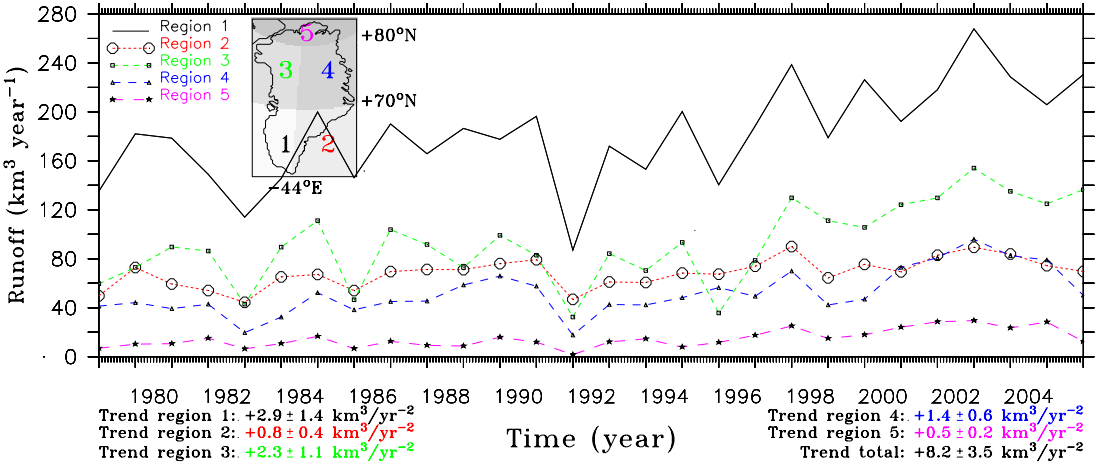

Fig. 17. Time series of run-off evolution for fives regions covering Greenland. The regions boundaries are –44° N in longitude and 70° N and 80° N respectively in latitude. These run-off rates include here the fresh water flux from both ice sheet and tundra on Greenland.

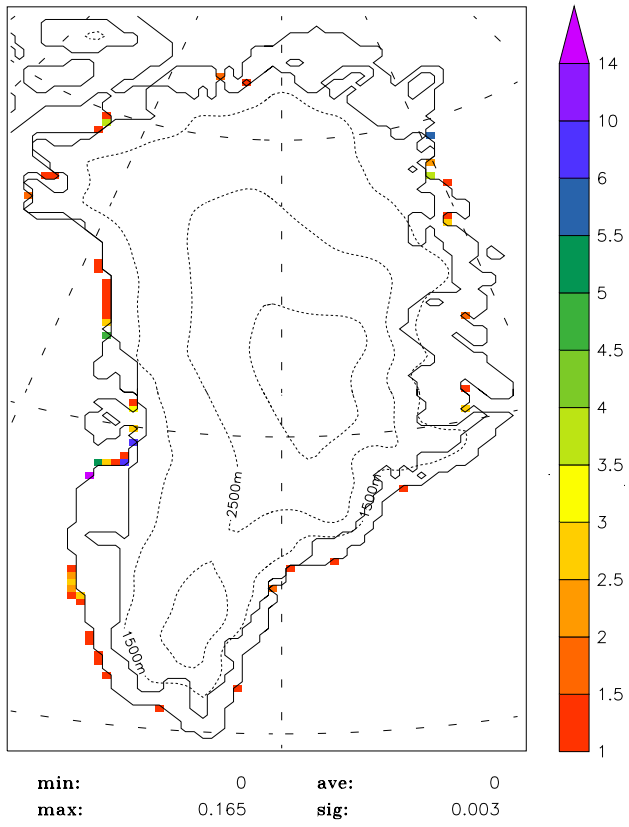

Fig. 18. Freshwater flux from run-off of the melt water and rainfall into the ocean for 2003. The freshwater fluxes have been obtained by a simple routing scheme based on the topography. Units are in 10^{-4} Sv.